scientific reports

Check for updates

OPEN

Energy evolution and damage characteristics of coal rock under graded cyclic loading and unloading with confining pressure

Zhongqian Chen, Shuang Dang✉, Chaolin Wang, Mingxuan Shen, Tao Wei & Qian Cao

This work conducts staged confining pressure cyclic loading and unloading (SCPLU) tests on coal rock to explore its energy evolution and damage features under complex stress states. A novel damage variable based on dissipated energy and enhanced modulus of elasticity is proposed. Results show that under low confining pressure, coal rock failure is minimally affected by cyclic unloading, with few micro-cracks. However, under high confining pressure, micro-cracks increase with rising confining pressure and unloading cycles. After each stage of loading and unloading, stress redistribution in coal rock causes micro-crack propagation, more dissipated energy, increased irreversible plastic deformation, and worsened damage. The damage variable based on dissipated energy and the improved modulus of elasticity has a high fitting degree of 0.998 with the damage evolution equation based on the Weibull distribution, which is superior to the improved modulus of elasticity method alone. The failure process of coal rock can be divided into five stages: compaction segment, elastic segment, crack instability development segment, crack instability propagation segment, and residual strength segment. This classification effectively characterizes the failure process of coal rock and provides a reference for further revealing the damage evolution mechanism of coal rock under complex stress paths.

Keywords Energy evolution, Coal rock, Graded cyclic loading and unloading with confining pressure, Damage variable

In the complex environment of geological tectonic activity and engineering disturbance[1–4], the processes of rock deformation and failure are extremely intricate[5–7]. The process is impacted by the rock material's inherent mechanical properties combined with other factors, including the stress path[8,9] and the evolution of micro-cracks and defects within the rock mass[10]. In underground coal mining, coal pillars in goaf areas are particularly influenced by mining disturbances[11–15], coal pillars experience cyclic loading and unloading processes, which can lead to instability and failure[16]. This causes the stress in the overlying strata to continuously shift towards the intact coal pillars, resulting in deformation and breakdown of coal rock[17–19]. Therefore, studying coal rock failure under SCPLU conditions is crucial for coal mine stability and safety.

The rock failure process is characterized by the generation, transformation, dissipation, and release of energy[20–23]. In recent years, as rock mechanics and damage mechanics have advanced, more scholars have begun to focus on the energy transformation mechanisms[18,24,25]. Triaxial cyclic loading and unloading experiments have been conducted on different types of rocks to explore the energy evolution during the cyclic process and to clarify the failure characteristics of rock[26–28]. Liu et al.[29] explored the connection between energy dissipation and crack propagation through triaxial cyclic loading and unloading tests on porous siltstone. Zhang et al.[30] studied the evolution laws of elastic strain energy and dissipated energy at different sampling depths of coal rock. Defining damage from the perspective of energy can reveal the failure characteristics of rock[31,32]. Peng et al.[33] redefined the damage variable on the basis of dissipated energy and analysed the energy evolution laws of multiple-defect sandstone samples with different defect lengths under uniaxial loading. Shen et al.[34] triaxial compression tests to develop a logistic-based dissipated energy equation and study coal damage features.

The stress path, initial confining pressure, unloading rate, and rock properties all impact the damage features in triaxial cyclic loading and unloading tests. Numerous researchers have carried out experimental investigations in these areas. Zhang et al.[35] performed tests on marble in various stress paths and found that failure modes and

College of Civil Engineering, Guizhou University, Huaxi District, Guiyang 550025, Guizhou, China. ✉email: sdang@gzu.edu.cn

energy storage differ between uniaxial and triaxial conditions. Zhao et al.[36] conducted unloading tests on rocks and concluded that higher initial confining pressures led to greater elastic energy, and dissipated energy. Guo et al.[37] explored the impact of the unloading rate on the energy evolution law of coal was investigated. The unloading rate is inversely proportional to the total work and the stored elastic strain energy. Zhang et al.[38] performed uniaxial tests on coal and sandstone, analyzing the energy evolution, finding that Coal stores less energy and dissipates more.

In summary, the characteristics of energy evolution in rock, influenced by many factors, can reflect the rock's failure process. Present studies primarily concentrate on how rock energy changes and its damage features behave under conditions of cyclic loading and unloading in both uniaxial and triaxial settings. The energy evolution and damage mechanisms of rock under SCPLU still need further investigation. During underground mining engineering and tunnel excavation processes, the original stress state of the surrounding rock is disrupted, resulting in stress redistribution. Consequently, the surrounding rock is subjected to a certain confining pressure. As mining and excavation progress, the goaf areas around the roadways continuously expand, the stress state of the surrounding rock undergoes constant changes, and the confining pressure also experiences a process of staged adjustment[39]. Moreover, the repeated loading caused by excavation, blasting, backfilling, and other operations can readily cause deformation and instability in the surrounding rock. Therefore, in this work, SCPLU tests are conducted on coal rock samples under different confining pressures to investigate the energy evolution characteristics and damage mechanisms of coal rock. A new method for calculating the damage variable based on dissipated energy and an improved modulus of elasticity is defined to describe the damage features during this process. This lays a theoretical groundwork for further exploring the failure mechanisms of coal rock under complex stress conditions from an energetic viewpoint.

Experimental materials and procedures

Test scheme

The testing equipment is a 1000-type stress-strain controlled triaxial shear permeability testing machine. The maximum axial pressure of the triaxial testing machine is 1000 KN, with a testable axial pressure range of 10–1000 kN. The upper limit of confining pressure is 60 MPa. Figure 1 shows the testing equipment.

Sample preparation

The coal rock samples were sourced from the Houwenjialiang Coal Mine in the Inner Mongolia Autonomous Region. The coal rock type is long-flame coal, and the mining depth is 65–70 m. The coal rock samples were made into standard cylindrical shapes, sized at 50 mm in diameter and 100 mm in length, conforming to the ISRM standard[40]. The ends of the coal rock samples were polished to be flat to ensure that they met the experimental requirements. The processed coal rock samples are shown in Fig. 2. Three coal rock samples, numbered MY-1, MY-2, and MY-3, were selected for the experiment. The samples underwent SCPLU testing at various confining pressures (3, 6, and 9 MPa) and the same unloading amplitude (1.5 MPa).

Stress paths during the test

The experimental process is shown in Fig. 3 and consists of three stages. In Stage I, the confining pressure is loaded to the preset value (3, 6 and 9 MPa) at a rate of 3 MPa/min, and the axial stress is loaded at the same rate. In Stage II, The axial stress is increased to 120% of the samples' uniaxial compressive strength (15 MPa) while the confining pressure remains constant. In Stage III, SCPLU begin. In each cycle, the confining pressure is reduced by 1.5 MPa from the maximum of the cycle for a duration of 30 min. A total of 30 cycles are conducted, with

Fig. 1. Model 1000 stress-strain controlled triaxial shear permeability testing apparatus.

Fig. 2. Coal rock samples.

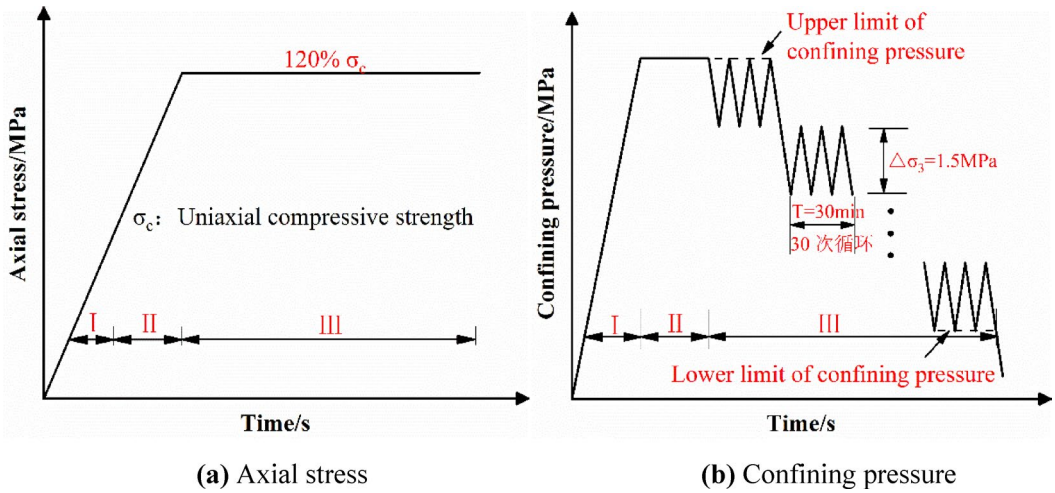

Fig. 3. Loading mode.

loading and unloading rates of 3 MPa/min, until failure of the sample and the loading and unloading process is stopped.

Results

Stress–strain characteristics

Figure 4 shows the relationship between the deviatoric stress–strain of coal rock samples. Coal rock is heterogeneous and contains a certain number of micro-cracks. When subjected to external forces, these micro-cracks continuously close, expand, and coalesce[41]. As shown in Fig. 4, before reaching the peak strength, he coal rock samples exhibit greater axial deformation than radial deformation, and the radial strain curves are almost coincident with the same slope. At the peak strength, the stress-strain curve of the sample does not have a distinct yield plateau under low confining pressure (σ_3 = 3 MPa). However, as σ_3 rises, the plasticity of the coal rock increases progressively, and the yield plateau becomes more pronounced.

After the peak strength, the ε_1 and ε_3 increase rapidly, with the ε_3 being significantly greater than the ε_1.When σ_3 = 3 MPa, the postpeak stress drop of the coal rock sample exceeds σ_3 = 6 MPa and σ_3 = 9 MPa, and the residual strength is lower. The analysis suggests that under SCPLU, a high confining pressure inhibits the propagation of micro-cracks within coal rock. These micro-cracks continuously close and open in localized areas, forming many micro-cracks. In contrast, under low confining pressure, micro-cracks are more likely to coalesce into rupture surfaces, thus exhibiting more distinct brittle characteristics. This indicates that confining pressure can enhance the ability of coal rock to resist deformation[42].

In addition, when σ_3 = 3 MPa, the failure pattern of coal rock is characterized by a mixture of shear and splitting failure. Specifically, a vertical splitting crack and an inclined rupture surface are formed on the surface of the sample. When the σ_3 is raised to 9 MPa, the dominant failure mode of the coal or rock shifts to shear failure. The end of the sample exhibited an inclined rupture surface, some micro-cracks formed in the vicinity of these rupture surfaces. Notably, with the σ_3 rises from 6 to 9 MPa, the quantity of micro-cracks near the rupture surfaces also rises, and the shape of the rupture surfaces becomes more tortuous and complex. High

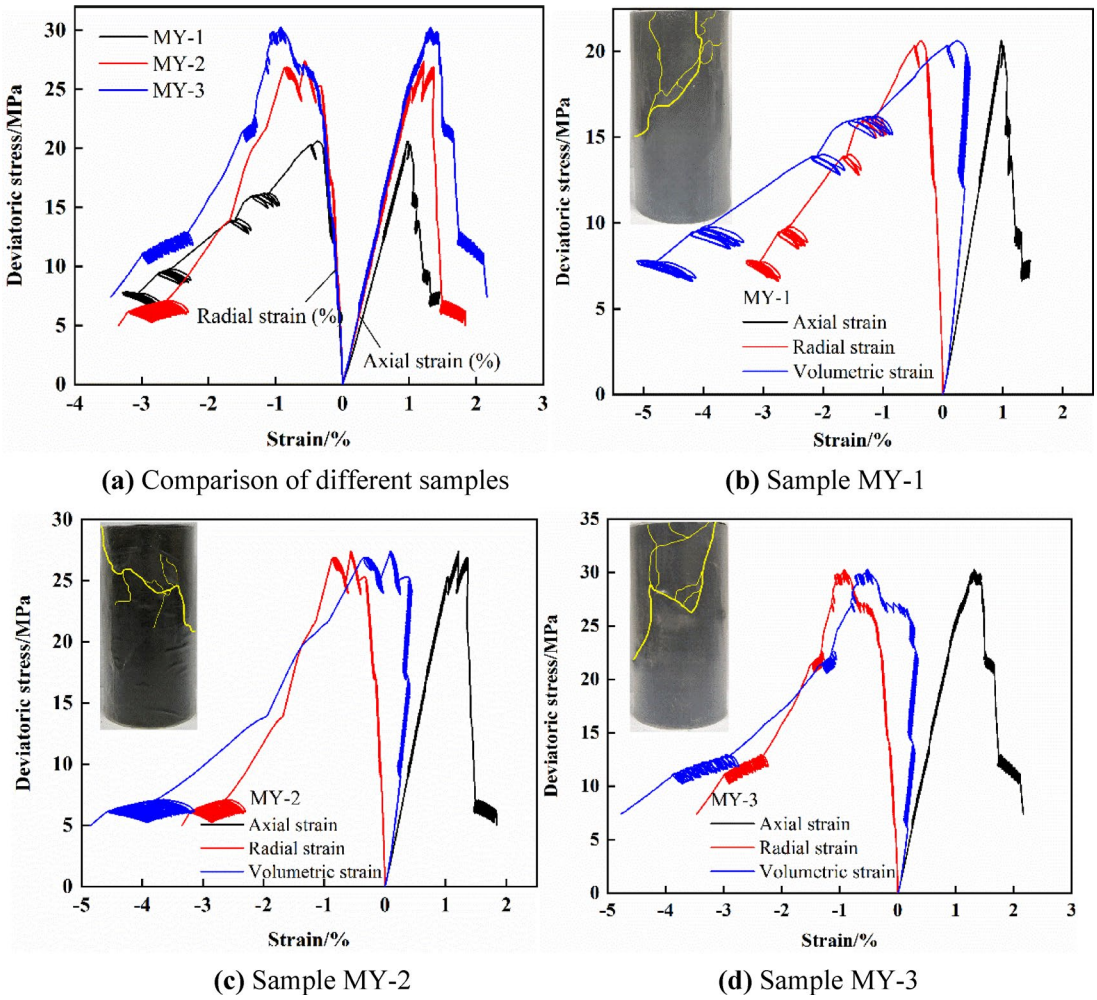

Fig. 4. Deviation stress–strain curves of coal rock.

confining pressure restricts crack coalescence, resulting in more cracks within the coal rock and more noticeable fragmentation features.

Figure 5 shows the confining pressure–strain curves of coal rock. During SCPLU, the hysteresis loop refers to the area formed by the non-coincidence of the loading and unloading curves, representing the dissipated energy[11]. With the increase cycles, the slopes of the hysteresis loops for MY-1, MY-2, and MY-3 increase, the range of strain variation for each cycle becomes larger, the area of the hysteresis loop increases, and the slopes of the loading and unloading curves decrease, energy dissipation rises.

As can be seen from Fig. 5a, the axial strain changes only slightly during each unloading stage, indicating that staged confining pressure unloading has a relatively minor impact on the axial direction. Figure 5b illustrates the variation pattern of radial strain with respect to confining pressure. The radial strain gradually increases as the number of unloading stages rises, and the range of change in radial strain during each unloading stage also gradually widens. This reflects continuous radial dilation during the unloading process. During the final unloading stage, the radial strain of the coal-rock increases significantly, ultimately leading to failure. The variation of volume strain with confining pressure in Fig. 5c also exhibits the same pattern.

Figure 5d illustrates the evolution of the hysteresis loop during the final unloading stage. The ranges of radial strain variation for MY-1, MY-2, and MY-3 are −0.004 to −0.033, −0.023 to −0.033, and −0.022 to −0.030, respectively. Moreover, with an increasing number of cycles, the confining pressure varies within a specific range, and crack propagation stabilizes. The area of the hysteresis loops no longer changes, indicating that the deformation under this level of confining pressure has stabilized. When the next cycle begins, the damage intensifies further, and plastic deformation continues to accumulate, ultimately leading to failure of the coal rock.

Analysis of the mechanical parameters of coal rock

To further analyse the relationship between the confining pressure and the mechanical parameters of coal rock, this study takes MY-2 as an example and draws a schematic diagram of the stage division of the deviatoric stress–strain curve of coal rock, as presented in Fig. 6, determine the characteristic stress points. The point at which the stress–strain curve has a relatively constant slope. The inflection point of the stress–strain curve

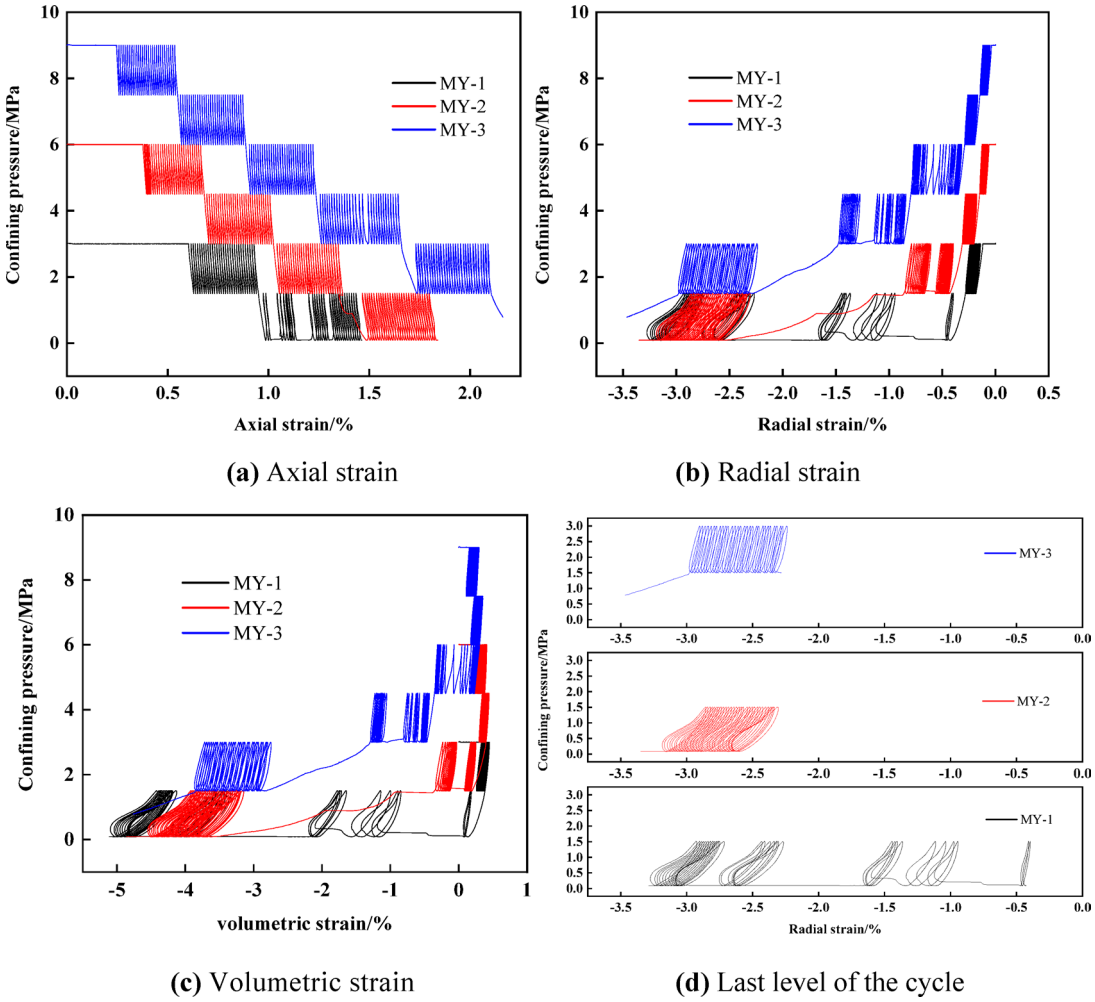

Fig. 5. Stress–strain curves of coal rock.

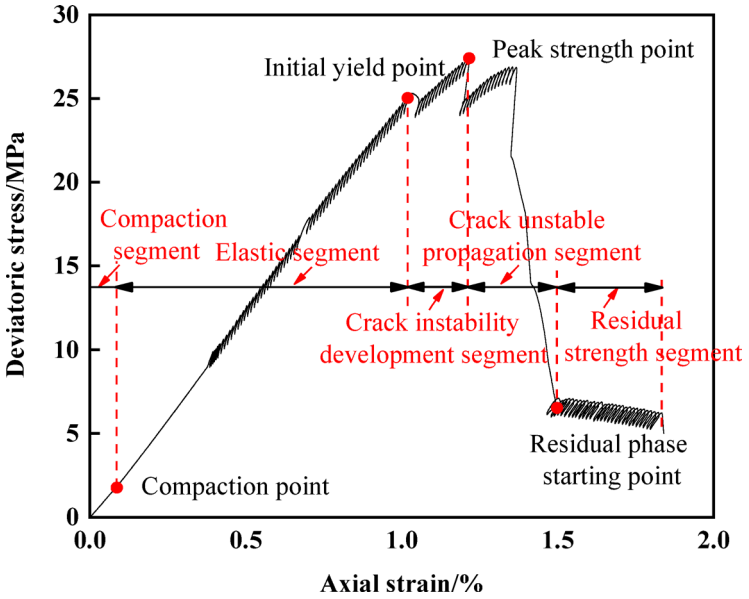

Fig. 6. Schematic diagram of the phase division for the deviatoric stress–strain curve of coal.

Sample	σ_3 (MPa)	σ_1^p (MPa)	σ_r (MPa)	ε_1^p (%)	ε_3^p (%)	ε_V^p (%)	E (GPa)	E_i (GPa)	E_p (GPa)	E_r (GPa)
MY-1	3	20.630	6.791	0.976	−0.368	0.383	2.197	2.141	2.011	0.367
MY-2	6	27.418	6.131	1.216	−0.561	0.466	2.557	2.525	2.047	0.476
MY-3	9	30.279	11.857	1.319	−0.918	0.647	2.633	2.611	2.185	0.557

Table 1. Results of coal rock testing.

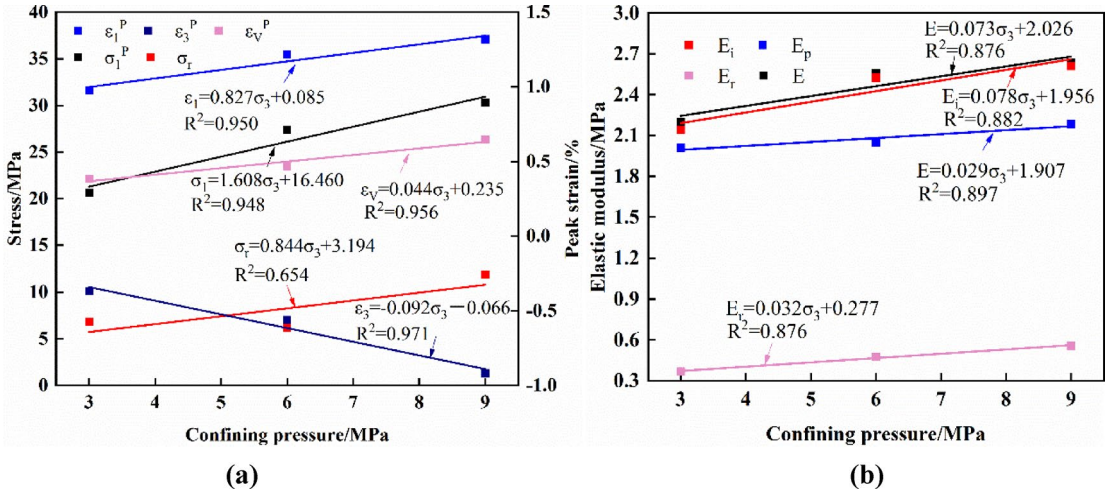

Fig. 7. (**a**) Relationships between the stress, peak strain, and confining pressure; (**b**) Relationships between the elastic modulus and confining pressure.

represents the initial yield point[43]. The peak strength point is when deviatoric stress reaches its maximum. The start of the residual stage is the onset of the postpeak plastic flow plateau[44].

Table 1 presents the results of the SCPLU tests, whereas Fig. 7 shows the relationships between the mechanical parameters of coal rock and the initial confining pressure. In Table 1 and Fig. 7, σ_1^p, σ_3 and σ_r represent the peak strength, confining pressure and residual strength; ε_V^p, ε_1^p and ε_3^p denote the peak volumetric strain, peak axial strain and peak radial strain; E is the elastic modulus (the slope of the elastic segment of the stress–strain curve); E_i, E_p and E_r represent the elastic moduli (tangent moduli) at the initial yield point, peak strength point, and beginning of the residual stage, respectively.

As the confining pressure increases from 3 to 9 MPa, the peak strength of the coal increases from 20.630 to 30.279 MPa, and the residual strength increases from 6.791 to 11.857 MPa. The elastic modulus also increases from 2.197 to 2.633 GPa. The elastic moduli at the initial yield point, peak strength point, and beginning of the residual stage all gradually increase, indicating a positive correlation with the confining pressure, which suggests that confining pressure can enhance the ultimate and residual load-bearing capacities of coal rock.

Energy evolution characteristics of coal rock

Energy calculation method

During rock deformation, the total energy is invariant. The work done by external forces equals the energy absorbed during loading, which can be described as[45,46]:

$$U = U_e + U_d \tag{1}$$

where U represents the total absorbed energy, U_e represents the stored elastic energy, and U_d represents the dissipated energy.

During the testing process, the sample is subjected to axial stress σ_1 and radial stresses σ_2 and σ_3. All three stresses work on the sample as it undergoes deformation. Thus, the total energy can be represented as[47]:

$$U = U_1 + U_2 + U_3 \tag{2}$$

where U_1 denotes the work performed by the axial stress, U_2 and U_3 are indicative of the work done by the radial stresses, and $U_2 = U_3$. Characterizing the total energy absorbed by coal rock as[29]:

$$U_N = U_N^e + U_N^d = U_{1,N} + 2 \times U_{3,N} \tag{3}$$

where U_N^e represents the elastic energy, U_N^d represents the dissipated energy, and $U_{1,N}$ and $U_{3,N}$ represent the axial strain energy and radial strain energy absorbed by the rock sample in the N-th cycle of loading and unloading, respectively.

The calculation of energy can be performed by determining the area of infinitesimal trapezoids, as shown in Fig. 8. The loading curve area, represented by the region CBB'C', is the axial (radial) strain energy absorbed $U_{1,N}(U_{3,N})$. The shaded area under the unloading curve, represented by the CDD'C' region, indicates the axial (radial) elastic energy released $U_{1,N}^e(U_{3,N}^e)$. The difference between these two areas represents the axial (radial) dissipated energy. The calculation methods for $U_{1,N}$, $U_{1,N}^e$, and $U_{1,N}^d$ are as follows[10,45]:

$$\begin{aligned} U_{1,N} &= \sum_{i=1}^{n} \frac{1}{2}[(\sigma_i)_1 + (\sigma_{i+1})_1]\,[(\varepsilon_i)_1 - (\varepsilon_{i+1})_1] \\ U_{1,N}^e &= \sum_{i'=1}^{n} \frac{1}{2}[(\sigma_i')_1 + (\sigma_{i+1}')_1]\,[(\varepsilon_i')_1 - (\varepsilon_{i+1}')_1] \\ U_{1,N}^d &= U_{1,N} - U_{1,N}^e \end{aligned} \tag{4}$$

The methods for calculating the $U_{3,N}$, $U_{3,N}^e$, and $U_{3,N}^d$ are as follows:

$$\begin{aligned} U_{3,N} &= \sum_{i=1}^{n} \frac{1}{2}[(\sigma_i)_3 + (\sigma_{i+1})_3][(\varepsilon_i)_3 - (\varepsilon_{i+1})_3] \\ U_{3,N}^e &= \sum_{i'=1}^{n} \frac{1}{2}[(\sigma_i')_3 + (\sigma_{i+1}')_3][(\varepsilon_i')_3 - (\varepsilon_{i+1}')_3] \\ U_{3,N}^d &= U_{3,N} - U_{3,N}^e \end{aligned} \tag{5}$$

For the N-th loading and unloading cycle, the elastic energy stored and the dissipated energy in coal rock can be expressed as:

$$\begin{aligned} U_N^e &= \sum_{i'=1}^{n} \frac{1}{2}[(\sigma_i')_1 + (\sigma_{i+1}')_1][(\varepsilon_i')_1 - (\varepsilon_{i+1}')_1] \\ &\quad + \sum_{i'=1}^{n}[(\sigma_i')_3 + (\sigma_{i+1}')_3][(\varepsilon_i')_3 - (\varepsilon_{i+1}')_3] \\ U_N^d &= U_N - \sum_{i'=1}^{n} \frac{1}{2}[(\sigma_i')_1 + (\sigma_{i+1}')_1][(\varepsilon_i')_1 - (\varepsilon_{i+1}')_1] \\ &\quad - \sum_{i'=1}^{n}[(\sigma_i')_3 + (\sigma_{i+1}')_3][(\varepsilon_i')_3 - (\varepsilon_{i+1}')_3] \end{aligned} \tag{6}$$

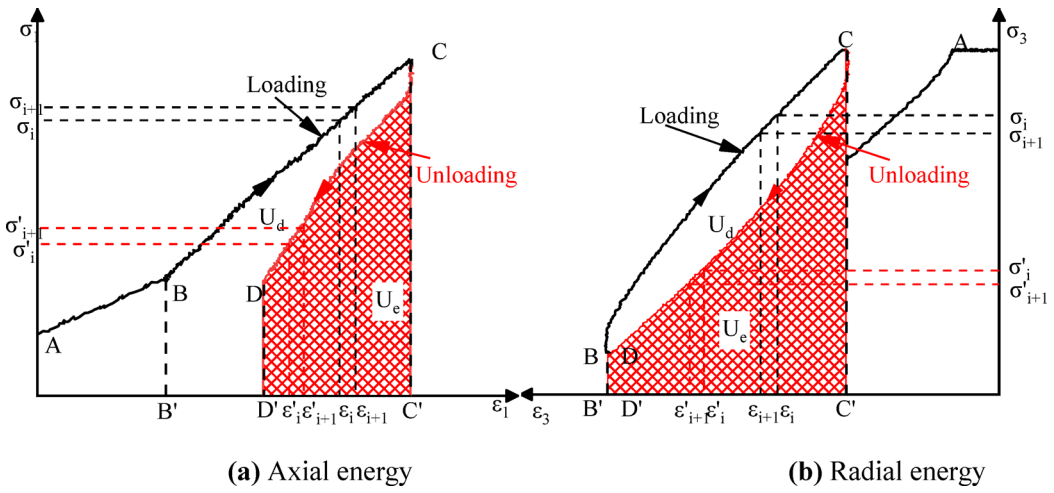

Fig. 8. Energy calculation diagram.

Analysis of elastic energy evolution

Rock failure involves by the generation, accumulation, transformation, and dissipation of energy. The stored elastic energy in rock can reflect its load-bearing capacity and degree of failure[48]. To analyse the evolution of elastic energy in coal rock under the condition of SCPLU, this paper calculates the elastic energy using the mentioned method. The axial elastic energy of coal rock in relation to the number of cycles is shown in Fig. 9a.

As cycles increases, the elastic energy initially increases gradually. When the sample approaches the final unloading stage, the elastic energy reaches its peak. As test continue, the axial elastic energy sharply decreases, followed by a slow decline. This behavior can be attributed to the initial SCPLU, during which fewer new cracks form and energy dissipation remains low. The energy produced during loading is mainly stored as elastic energy in coal rock, causing a gradual increase in axial elastic energy. As cycles increases, many new cracks continuously form within the sample, gradually expanding and interconnecting. During this process, the elastic energy within the coal rock sample is rapidly dissipated, leading to a sharp decrease in axial elastic energy. Moreover, during the transition between each cycle, the stress state is redistributed. This abrupt change in the stress state causes a reallocation and release of energy, thereby inducing a sudden change in elastic energy.

Figure 9b shows the relationship between the radial elastic energy of coal rock and cycles under varying confining pressures. As cycles grows, the radial elastic energy initially declines gradually, reaches a minimum value, and then slowly increases, with an overall relatively gentle trend. The reason for this is that during the initial phases of cyclic unloading, the deformation observed in coal rock is primarily due to the compression of internal voids and fractures. This leads to relatively minor radial strains and a progressive reduction in radial strain energy. As cycles increases, the irreversible strain increases sharply, and the cracks expand rapidly, causing an increase in the radial elastic energy.

The energy storage limit U_e^{max} can indicate the energy accumulation capacity of rock. the correlation between rock's energy storage potential and confining pressure is defined as $Y = A\sigma_3 + B$[25], where Y represents the upper limit of rock energy storage, A is the impact factor of confining pressure on U_e^{max}. To explore the connection between σ_3 and the U_e^{max} of coal rock, this study generates a scatter plot with confining pressure on the horizontal axis and maximum elastic energy on the vertical axis, and performs a linear fit. The correlation between σ_3 and U_e^{max} is depicted in Fig. 10. When the σ_3 are 3, 6 and 9 MPa, the maximum elastic energy stored in coal rock are 0.0178, 0.03137 and 0.04076 MJ/m^3. When σ_3 =9 MPa , the energy storage limit is 1.299 times greater than that at 6 MPa and 2.283 times greater than that at 3 MPa. Additionally, the coefficient of determination (R^2) for the fit between confining pressure and energy storage limit is 0.989, indicating a positive correlation between confining pressure and energy storage limit.

To analyse the energy variation under each stress state, this paper takes the average energy as the vertical coordinate and obtains the average energy at different cycle numbers, as shown in Fig. 11. Since the unloading process of MY-1 has only two stages, it cannot reflect the variation law of average energy. Therefore, it is not analysed in this paper. Figure 10 shows that with increasing cycles, the U and total energy of MY-2 first rise but then gradually fall. Damage to coal rock results in the dissipated energy reaching a maximum. The elastic energy is converted into dissipated energy, which facilitates crack expansion and penetration. The evolution of the average energy of MY-3 is similar to that of MY-2. When σ_3 = 9 MPa, the coal rock is damaged in the fourth cycle, with the average dissipated energy peaking.

Analysis of dissipated energy evolution

The ratio of energy dissipation reflect the degree of internal damage in rock[49]. The ratio of energy dissipation for the N-th cycle is given by:

$$\eta_N = \frac{U_N^{\mathrm{d}}}{U_N} = 1 - \frac{U_N^{\mathrm{e}}}{U_N} \tag{7}$$

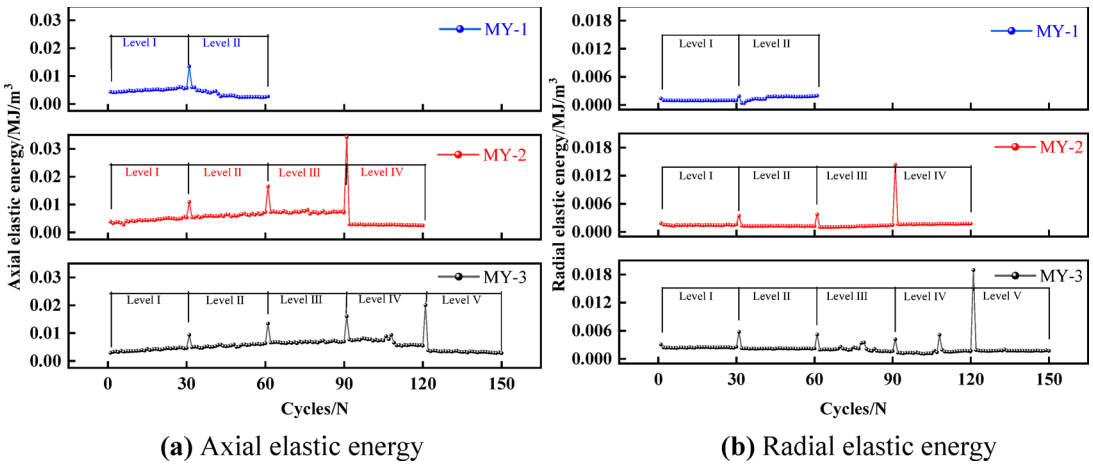

(a) Axial elastic energy **(b)** Radial elastic energy

Fig. 9. Evolution curves of the elastic energy in coal rock under different confining pressures.

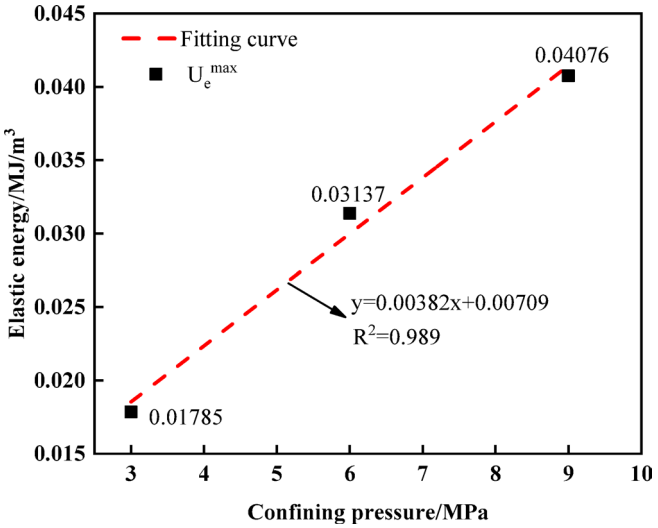

Fig. 10. Relationship between the energy storage limit and confining pressure.

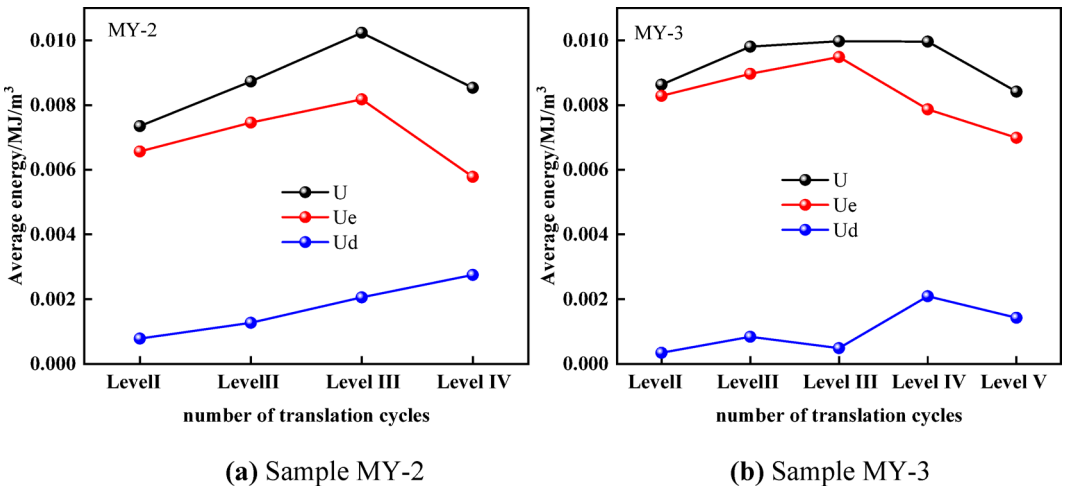

Fig. 11. Average energy at different cycle numbers.

The relationship between strain energy, number of cycles, and the ratio of dissipated energy is shown in Fig. 12. In the early SCPLU, coal rock deformation is mainly due to micro-crack compression without new crack generation. Thus, loading energy is primarily stored as elastic energy in coal rock[50]. As cycles increase, total energy and dissipated energy keep rising, and the share of dissipated energy also rises until it reaches a maximum at a certain point. During this process, the elastic energy remains almost constant due to the lack of new crack formation consuming the dissipated energy. In the postpeak stage, the cracks fully penetrate to form rupture surfaces. The proportion of dissipated energy sharply increases as the total energy continuously decreases. Elastic energy stored within coal rock is continuously released and converted into dissipated energy, which drives the expansion, penetration, and failure of cracks. As shown in Fig. 12d, under the same number of cycles, the higher the confining pressure is, the smaller the energy dissipation ratio. A higher confining pressure inhibits crack propagation, reducing the brittleness of coal and increasing its ductility. This causes an elevation in the elastic energy stored within coal rock and a rise in total energy, thus diminishing the energy dissipation ratio.

Discussion

Definition of the damage variable based on dissipated energy and the improved elastic modulus method

The essence of rock failure is energy instability[51]. To describe the damage features of rock, Xie et al.[52] proposed a definition of damage for elastic-plastic materials that considers the influence of irreversible plastic deformation under one-dimensional conditions:

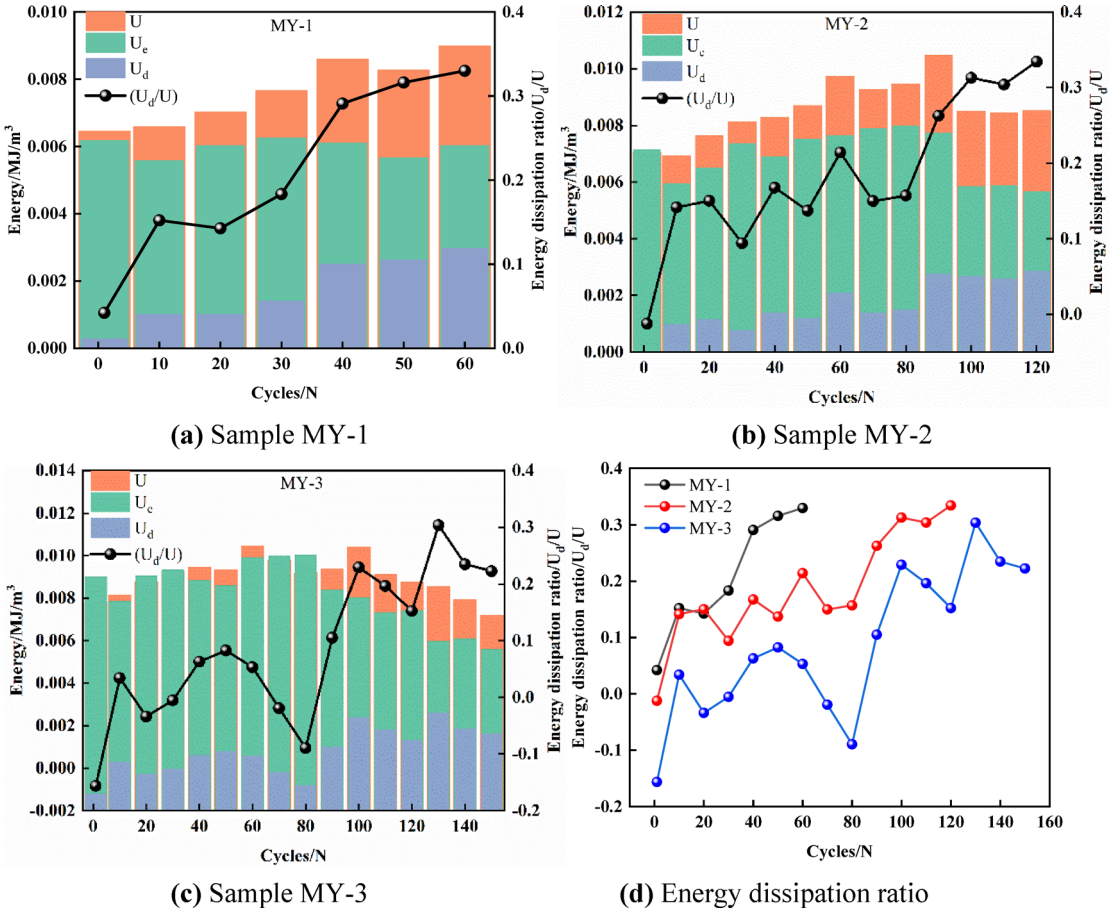

Fig. 12. Strain energy—number of cycles—energy consumption ratio of coal rock.

$$D = 1 - \frac{\varepsilon - \varepsilon'}{\varepsilon}\left(\frac{E'}{E}\right) \tag{8}$$

where D represents the damage variable; ε' and ε represent the residual plastic deformation after unloading and the axial strain, respectively; and E' and E represent the unloading stiffness and the initial elastic modulus of the elastoplastic damaged material, respectively.

Cyclic loading and unloading under uniaxial conditions can be described by this definition. To better describe the evolution of damage variables in coal rock during SCPLU tests, this paper introduces a new method for calculating damage variables, using the improved elastic modulus method. This method takes into account both axial and radial damage as well as dissipated energy. Let N represent the number of cycles; the axial damage variable is expressed as:

$$D_{1N} = 1 - \frac{\varepsilon_{1N} - \varepsilon'_{1N}}{\varepsilon_{1N}}\left(\frac{E'_N}{E}\right) \tag{9}$$

where D_{1N} represents the axial damage variable at the N-th cycle and where ε'_{1N} and ε_{1N} represent the residual axial plastic deformation and axial strain after unloading, respectively, where $\varepsilon'_{1N} = \varepsilon_{1(N+1)} - \varepsilon_{1N}$, and E'_N, E represent the unloading stiffness of the elastoplastic damaged material and the initial elastic modulus at the N-th cycle, respectively. Similarly, The radial damage variable is given by:

$$D_{3N} = 1 - \frac{\varepsilon_{3N} - \varepsilon'_{3N}}{\varepsilon_{3N}}\left(\frac{E'_N}{E}\right) \tag{10}$$

where D_{3N} represents the radial damage variable at the N-th cycle and where ε'_{3N} and ε_{3N} are the residual radial plastic deformation and radial strain after unloading, respectively, where $\varepsilon'_{3N} = \varepsilon_{(3N+1)} - \varepsilon_{3N}$. The total damage variable is given by:

$$D_N = \frac{U_{d1}}{U_d} D_{1N} + \frac{U_{d3}}{U_d} D_{3N}$$
$$D_N = \frac{U_{d1}}{U_d}\left[1 - \frac{\varepsilon_{1N} - \varepsilon'_{1N}}{\varepsilon_{1N}}\left(\frac{E'_N}{E}\right)\right] + \frac{U_{d3}}{U_d}\left[1 - \frac{\varepsilon_{3N} - \varepsilon'_{3N}}{\varepsilon_{3N}}\left(\frac{E'_N}{E}\right)\right] E \tag{11}$$

where U_d represents the total dissipated energy, U_{d1} represents the total axial dissipated energy, and U_{d3} represents the total radial dissipated energy. D_N is the damage variable of the sample at the N-th cycle. When D_N=0, the sample is intact; when D_N=1, the sample has failed. Larger D_N values indicate more severe rock sample damage.

Coal rock is a brittle material. In accordance with the energy-based statistical damage constitutive model, it is assumed that the strength of rock units obeys the Weibull distribution[53], with the probability density function given by:

$$P(\varepsilon) = \frac{m}{F}\left(\frac{\varepsilon}{F}\right)^{m-1} \exp\left[-\left(\frac{\varepsilon}{F}\right)^m\right] \tag{12}$$

where m and F are the parameters that define the shape and scale of the distribution, and are associated with the material properties of the rock. Therefore, the count of rock elements that fail at a strain of ε is given by:

$$n(\varepsilon) = N\int_0^{\varepsilon} P(x)dx = N\left\{1 - exp\left[-\left(\frac{\varepsilon}{F}\right)\right]^m\right\} \tag{13}$$

In the formula, N represents the total elements. The damage variable is defined as the proportion of failed elements to the total elements, the damage evolution equation for coal rock is obtained as[54]:

$$D = \frac{n}{N} = 1 - exp\left[-\left(\frac{\varepsilon}{F}\right)\right]^m \tag{14}$$

To demonstrate that this method can better depict the damage characteristics of coal rock during SCPLU, this paper compares the fitting degrees of the damage variables obtained via three different damage calculation methods—calculating damage via radial strain, calculating damage via axial strain, and the new damage variable calculation method—with the damage evolution equation. The higher the fitting degree is, the more accurate the damage calculation method is. For convenience in calculation and comparison, the radial strain is taken as a positive value during the calculations.

Figure 13 shows the fitting degree of the damage evolution equation under different damage calculation methods. D represents the damage variable defined in this paper, whereas D_1 and D_3 are the damage variables defined by the improved elastic modulus method. where ε_1 and ε_3 are the axial and radial strains used for fitting the damage evolution equation, respectively. As shown in Fig. 13 and Table 2, the damage variable defined by the combination of ε_1, ε_3, and dissipated energy has a significantly greater degree of fit with the damage evolution equation than the other methods of calculating damage. The coefficient of determination R^2 is above 0.983 in all cases, with the highest value reaching 0.998. Therefore, the damage evolution equation established by combining the principle of dissipated energy with the improved elastic modulus method can effectively describe the damage evolution law during the deformation and failure process of coal rock under SCPLU.

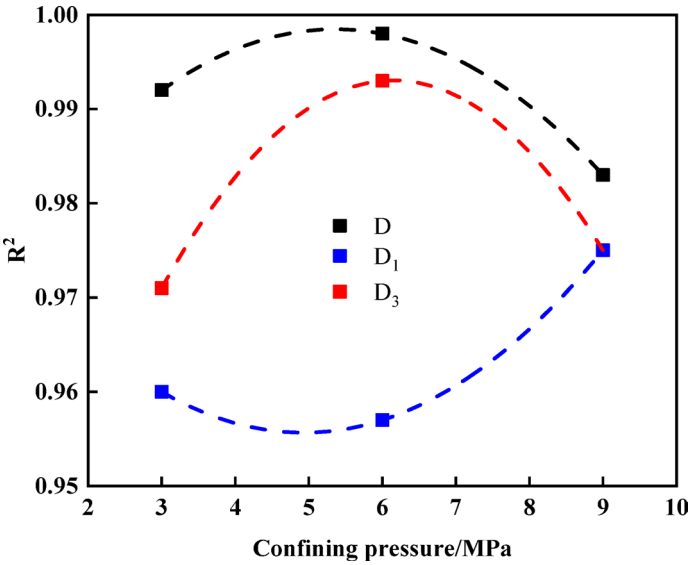

Fig. 13. Goodness of fit for damage evolution equations under different damage calculation methods.

Damage calculation method	R^2		
	MY-1	MY-2	MY-3
D	0.992	0.998	0.983
D_1	0.960	0.957	0.975
D_3	0.971	0.993	0.975

Table 2. Goodness of fit for damage evolution equations under different damage calculation methods.

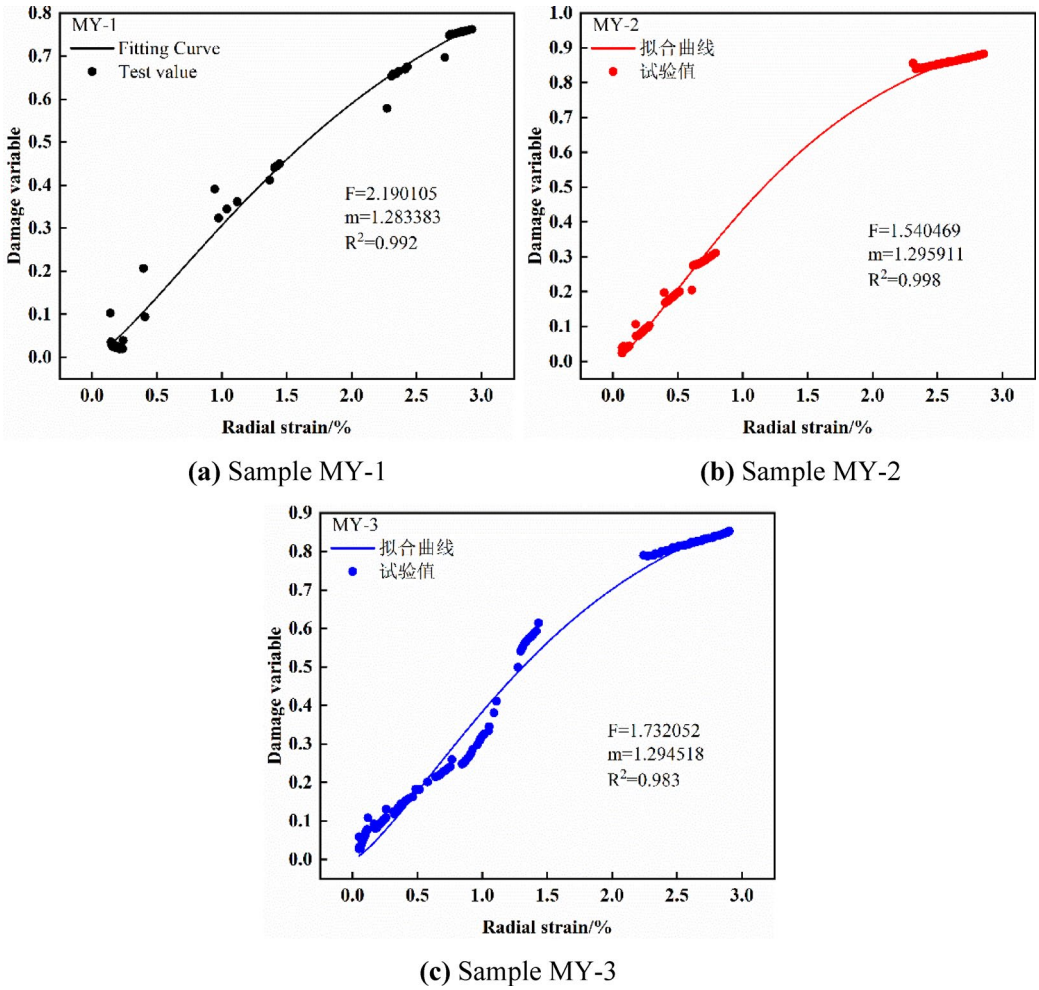

Fig. 14. Diagram of the fitting curves for the damage variable.

Figure 14 shows the fitting curves of coal rock damage evolution. As shown in Fig. 14a–c, in early SCPLU, the coal rock sample exhibits minimal radial deformation, and damage variable gradually increases with increasing radial strain. As unloading continues, the radial strain keeps increase, and when it increases to a certain level, both the radial strain and the damage variable increase sharply, followed by the failure of the sample. The failure of coal rock involves continuous damage accumulation, which leads to sudden failure when reached a certain threshold.

Damage evolution process

Figure 15 shows the damage evolution curves of coal rock, the SCPLU process consists of five stages.

Stage One: At the beginning of the cycle, the damage variable of the coal rock is not zero. This indicates that the coal rock sample already had some micro-cracks before the test started. The closure of these micro-cracks uses up some energy, which is why the initial damage variable is relatively large.

Stage Two: This stage is the elastic stage, where the micro-cracks are relatively stable and the change in the damage variable is not significant.

Stage Three: This is the unstable development stage of micro-cracks. The micro-cracks begin to expand, leading to a noticeable increase in the damage variable.

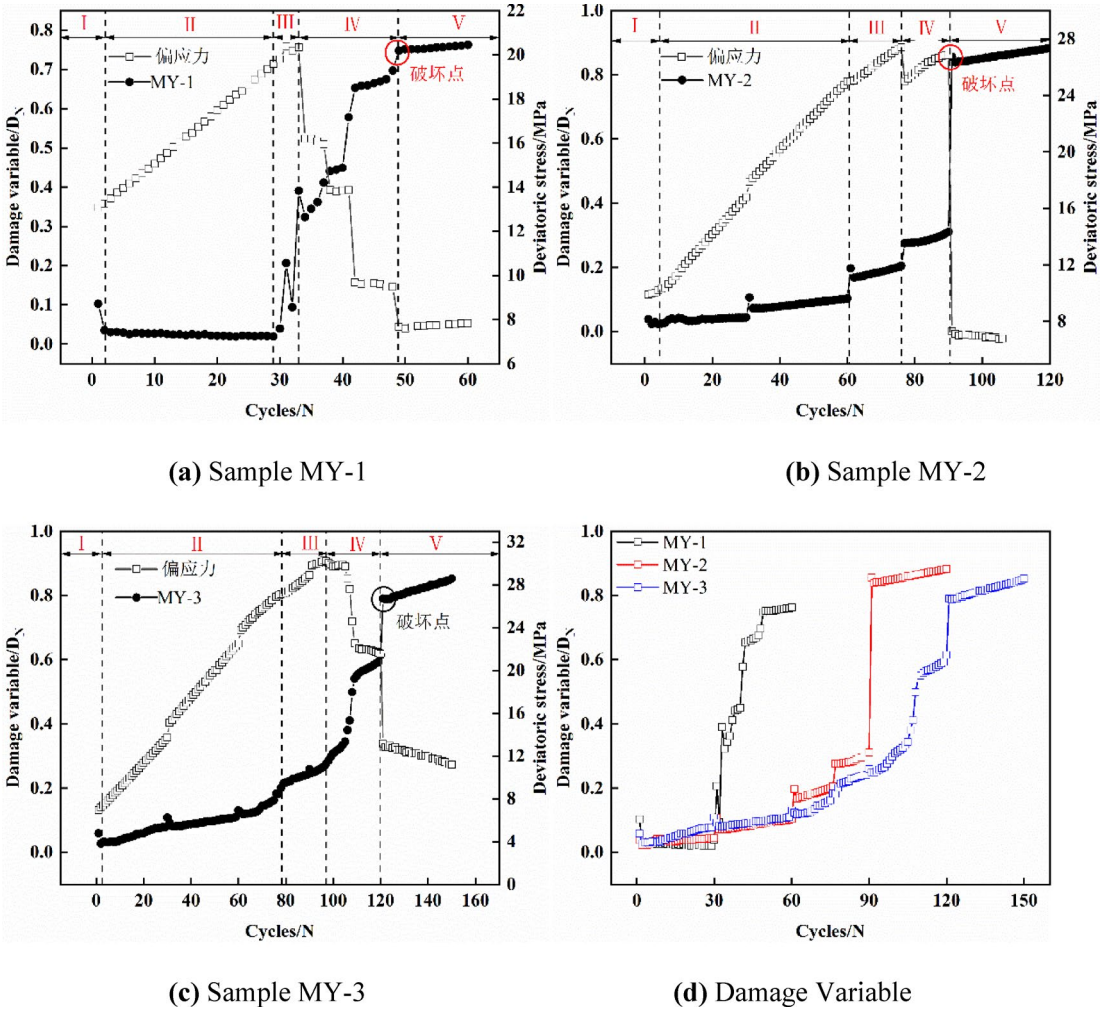

Fig. 15. Diagram of the damage evolution curves of coal rock.

Stage Four: This is the unstable expansion stage, where the damage variable increases sharply. Damage accumulates continuously, and the cracks continue expanding and coalescing, eventually leading to failure of the coal sample.

Stage Five: This is the residual strength stage, the internal state of the coal rock remains relatively stable, with insignificant changes in the damage variable.

Overall, the damage variable increases with the increasing number of cycles. During the transition from the end of one cycle to the beginning of the next, the damage variable experiences a sudden change. After the next cycle, it begins to increase steadily again. This is because the abrupt drop in confining pressure causes the energy stored in the coal sample to be rapidly released, causing rapid crack expansion and a continuous increase in damage. Once the next cycle begins, the coal rock stabilizes and the increase in the damage variable becomes more stable. At the same number of cycles, coal rock samples under high confining pressure tend to have a lower damage variable than those under low confining pressure. This is because high confining pressure suppresses crack propagation, resulting in a lower damage variable. This finding indicates that the damage variable defined in this paper can effectively characterize the failure process of rock during SCPLU.

To explore the link between the proportion of dissipated energy at the failure point of coal rock and the initial confining pressure, the failure point of the coal rock sample is determined as the point following the sudden change in the damage variable. The dissipated energy ratio versus confining pressure at this point is shown in Fig. 16. A clear linear relationship is observed between these two variables, with a fitting coefficient R^2 of 1. The proportion of dissipated energy at the failure point of the coal rock sample decreases as the confining pressure increases. This further shows that under SCPLU conditions, higher confining pressure restrains coal rock failure and boosts their load-bearing capacity.

The study is subject to several limitations. First, the experiments were conducted solely on laboratory-scale coal samples, neglecting potential field-scale effects and material heterogeneity. Second, the SCPLU path employed is relatively simplified and thus fails to fully capture the dynamic disturbances inherent to real mining-induced stress evolutions. Third, although the newly proposed damage variable exhibits high fitting accuracy, it

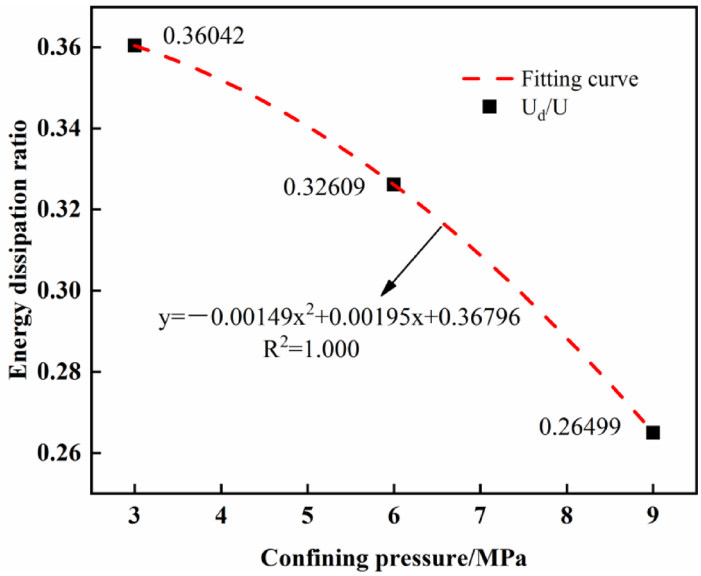

Fig. 16. Graph of the relationship between the confining pressure and the proportion of dissipated energy at the abrupt change in the coal rock damage variable.

has not been systematically validated across multiple rock types; its broader applicability therefore remains to be confirmed.

Conclusion

This study conducted SCPLU tests on coal rock samples, defined a new method for calculating damage variables, and analysed the energy evolution and damage characteristics of coal rock. The conclusions are as follows:

1. In the SCPLU tests, coal rock mainly undergoes splitting failure under low confining pressure, and cyclic loading has minimal impact on the failure mode. Under high confining pressure, shear failure is dominant, and the number of micro-cracks around the rupture surface grows as the confining pressure and the number of cycles increase.
2. In the SCPLU tests, when one cycle of loading and unloading ends and the next cycle begins, stress redistribution occurs within the coal rock. This leads to crack propagation, increased dissipated energy, increased irreversible plastic deformation, and further intensified damage.
3. The damage variable calculation method, defined based on dissipated energy and the improved elastic modulus approach, demonstrates a fitting degree of 0.998 with the damage evolution equation, outperforming the improved elastic modulus method alone. This method can divide the failure process of coal rock into five stages: the compaction stage, elastic stage, unstable crack development stage, unstable crack propagation stage, and residual strength stage.

Data availability

Data will be made available on reasonable request to author Shuang Dang (sdang@gzu.edu.cn).

Received: 11 July 2025; Accepted: 17 September 2025
Published online: 23 October 2025

References

1. Lu, X., Qin, R., Dong, C. & Fan, C. Damage characteristics and energy evolution of bituminous sandstones under different cyclic amplitudes. *Appl. Sci.* **13**, 7340 (2023).
2. Zhao, Y., He, P., Zhang, Y. & Wang, C. A new criterion for a toughness-dominated hydraulic fracture crossing a natural frictional interface. *Rock Mech. Rock Eng.* **52**, 2617–2629 (2019).
3. Zhang, M. et al. Study of borehole stability of volcanic rock formation with the influence of multiple factors. *J. Pet. Explor. Prod. Technol.* **14**, 3367–3382 (2024).
4. Fan, Z., Song, X., Wang, D., Ayasrah, M. T. & Li, S. Poroelastic solutions of a semipermeable borehole under nonhydrostatic in situ stresses within transversely isotropic media. *Int. J. Geomech.* **25** (2025).
5. Wang, D. et al. Study on stability and control of surrounding rock in the large section stopping space with extra-thick coal seam. *Alex. Eng. J.* **117**, 205–220 (2025).
6. Gao, R., Kuang, T., Meng, X. & Huo, B. Effects of ground fracturing with horizontal fracture plane on rock breakage characteristics and mine pressure control. *Rock Mech. Rock Eng.* **54**, 3229–3243 (2021).
7. Gao, R. et al. Ground fracturing of multi-strata for strong ground pressure control in extra-thick coal seams with hard roofs: numerical simulation and case study. *Eng. Fract. Mech.* **303**, 110129 (2024).
8. Zhao, Y., Wang, C. L. & Bi, J. Analysis of fractured rock permeability evolution under unloading conditions by the model of elastoplastic contact between rough surfaces. *Rock Mech. Rock Eng.* **53**, 5795–5808 (2020).

9. Dang, S., Yang, Z., Zhao, Y., Wang, C. & Bi, J. Experimental study of microwave thawing on the ln2 frozen coals for enhancing coalbed methane extraction. *Int. J. Coal Sci. Technol.* **12**, 17–51 (2025).
10. Liu, Y., Dai, F., Dong, L., Xu, N. & Feng, P. Experimental investigation on the fatigue mechanical properties of intermittently jointed rock models under cyclic uniaxial compression with different loading parameters. *Rock Mech. Rock Eng.* **51**, 47–68 (2018).
11. Ding, Z. W., Jia, J. D., Tang, Q. B. & Li, X. F. Mechanical properties and energy damage evolution characteristics of coal under cyclic loading and unloading. *Rock Mech. Rock Eng.* **55**, 4765–4781 (2022).
12. Jin, J. et al. Mechanical properties and compression damage characteristics of coal gangue-filled backfill cemented by fly ash modified self-consolidating grouts. *Case Stud. Constr. Mater.* **22**, e04687 (2025).
13. Jin, J. et al. Preparation of self-consolidating cemented backfill with tailings and alkali activated slurry: Performance evaluation and environmental impact. *Constr. Build. Mater.* **438**, 137088 (2024).
14. Zhang, M., Liang, L. & Liu, X. Analysis of the influence of different rock shear failure criteria on wellbore collapse pressure. *Chin. J. Rock Mech. Eng.* **36**(S1), 3485–3491 (2017).
15. Zhang, M. et al. The modification of Mohr-Coulomb criteria based on shape function and determination method of undetermined parameters. *Mech. Mater.* **185**, 104772 (2023).
16. Dang, S. et al. Strain evolution and fatigue damage characteristics analysis of sandstones during multi-level triaxial cyclic loading and unloading under varying stress limits. *Rock Mech. Rock Eng.* **56**, 2649–2671 (2023).
17. Zhang, K. et al. Study on the energy evolution mechanism of coal and rock with impact tendency under different strain rates. *Sci. Rep.* **13**, 13773 (2023).
18. Zhao, Y. et al. Energy evolution characteristics of sandstones during confining pressure cyclic unloading conditions. *Rock Mech. Rock Eng.* **56**, 953–972 (2023).
19. Zhang, M. et al. Influence of multi-planes of weakness on unstable zones near wellbore wall in a fractured formation. *J. Nat. Gas Sci. Eng.* **93**, 104026 (2021).
20. Ma, B. et al. Experimental investigation into influence of surrounding rock on strainburst: Insight from failure process and energy partition. *Int. J. Rock Mech. Min. Sci.* **175**, 105685 (2024).
21. Zhao, Y., Wang, C., Zhang, Y. & Liu, Q. Experimental study of adsorption effects on shale permeability. *Natural Resources Research (New York, N.Y.)* **28**, 1575–1586 (2019).
22. Zhao, Y., Zhang, Y., Wang, C. & Liu, Q. Hydraulic fracturing characteristics and evaluation of fracturing effectiveness under different anisotropic angles and injection rates: an experimental investigation in absence of confining pressure. *J. Nat. Gas Sci. Eng.* **97**, 104343 (2022).
23. Yang, D., Hu, J. & Ding, X. Analysis of energy dissipation characteristics in granite under high confining pressure cyclic load. *Alex. Eng. J.* **59**, 3587–3597 (2020).
24. Xin, T. et al. Study on deformation characteristics and damage evolution of water-bearing coal under cyclic loading. *Results Eng.* **27**, 105906 (2025).
25. Zhang, Y. et al. Strain energy evolution characteristics and mechanisms of hard rocks under true triaxial compression. *Eng. Geol.* **260**, 105222 (2019).
26. Guo, J. et al. Experimental investigation of nonlinear energy evolution and failure characteristics of granite under different water content states. *Geofluids* **2022**, 1–21 (2022).
27. Lv, Y. et al. Mechanical and degradation properties of rock under triaxial loading-unloading stresses: comparative insights into coal and sandstone. *Int. J. Rock Mech. Min. Sci.* **190**, 106102 (2025).
28. Zhang, M. et al. Parametric sensitivity study of wellbore stability in transversely isotropic medium based on polyaxial strength criteria. *J. Pet. Sci. Eng.* **197**, 108078 (2021).
29. Liu, Z. et al. Characteristics and association mechanism of energy dissipation and crack development in siltstone under triaxial cyclic loading and unloading. *Rock Mech. Rock Eng.* (2024).
30. Zhang, A. et al. Mechanical properties and energy characteristics of coal at different depths under cyclic triaxial loading and unloading. *Int. J. Rock Mech. Min. Sci.* **161**, 105271 (2023).
31. Huang, K., Zha, F., Kang, B., Sun, X. & Su, J. An energy-based damage model for red-bed sandstones subjected to drying–wetting cycles. *Géotech. Lett.* **11**, 215–220 (2021).
32. Wang, C., He, B., Hou, X., Li, J. & Liu, L. Stress–energy mechanism for rock failure evolution based on damage mechanics in hard rock. *Rock Mech. Rock Eng.* **53**, 1021–1037 (2020).
33. Peng, Y., Zhou, C., Fu, C., Zhong, Z. & Wang, J. Study on energy damage evolution of multi-flaw sandstone with different flaw lengths. *Theor. Appl. Fract. Mech.* **132**, 104469 (2024).
34. Shen, R., Wang, X., Li, H., Gu, Z. & Liu, W. Brittleness characteristics and damage evolution of coal under true triaxial loading based on the energy principle. *Nat. Resour. Res.* **33**, 421–434 (2024).
35. Zhang, L. et al. Energy evolution analysis and failure criteria for rock under different stress paths. *Acta Geotech.* **16**, 569–580 (2021).
36. Zhao, G., Dai, B., Dong, L. & Yang, C. Energy conversion of rocks in process of unloading confining pressure under different unloading paths. *Trans. Nonferrous Met. Soc. China* **25**, 1626–1632 (2015).
37. Guo, H., Sun, Z., Ji, M., Wu, Y. & Nian, L. An investigation on the impact of unloading rate on coal mechanical properties and energy evolution law. *Int. J. Environ. Res. Public Health* **19**, 4546 (2022).
38. Zhang, A. et al. Mechanical responses in rocks with different lithologies under mining loading–unloading: An insight by energy damage and ultrasonic characterization. *Rock Mech. Rock Eng.* **57**, 10047–10069 (2024).
39. Fan, L., Gao, J., Du, X. & Wu, Z. Spatial gradient distributions of thermal shock-induced damage to granite. *J. Rock Mech. Geotech. Eng.* **12**, 917–926 (2020).
40. Ulusay, R. *The ISRM Suggested Methods for Rock Characterization, Testing and Monitoring: 2007–2014* (Springer, Berlin, 2015).
41. Peng, K., Zhou, J., Zou, Q., Zhang, J. & Wu, F. Effects of stress lower limit during cyclic loading and unloading on deformation characteristics of sandstones. *Constr. Build. Mater.* **217**, 202–215 (2019).
42. Meng, Q. et al. Effects of confining pressure and temperature on the energy evolution of rocks under triaxial cyclic loading and unloading conditions. *Rock Mech. Rock Eng.* **55**, 773–798 (2022).
43. Shengqi, Y., Yang, J., Feng, G. & Gui, Y. Strength, Deformability and x-ray micro-ct observations of deeply buried marble under different confining pressures. *Rock Mech. Rock Eng.* **49**, 4227–4244 (2016).
44. Zhang, J. & Zhou, X. AE event rate characteristics of flawed granite: from damage stress to ultimate failure. *Geophys. J. Int.* **222**, 795–814 (2020).
45. Meng, Q., Zhang, M., Han, L., Pu, H. & Nie, T. Effects of acoustic emission and energy evolution of rock specimens under the uniaxial cyclic loading and unloading compression. *Rock Mech. Rock Eng.* **49**, 3873–3886 (2016).
46. Pan, C. et al. Fractal characteristics and energy evolution analysis of rocks under true triaxial unloading conditions. *Fractal Fract.* **8**, 387 (2024).
47. Yan, Z. et al. A novel application of strain energy for fracturing process analysis of hard rock under true triaxial compression. *Rock Mech. Rock Eng.* **52**, 4257–4272 (2019).
48. Zhang, M., Meng, Q. & Liu, S. Energy evolution characteristics and distribution laws of rock materials under triaxial cyclic loading and unloading compression. *Adv. Mater. Sci. Eng.* **2017**, 1–16 (2017).
49. Li, D., Sun, Z., Xie, T., Li, X. & Ranjith, P. G. Energy evolution characteristics of hard rock during triaxial failure with different loading and unloading paths. *Eng. Geol.* **228**, 270–281 (2017).

50. Zhao, K. et al. Energy evolution of brittle granite under different loading rates. *Int. J. Rock Mech. Min. Sci.* **132**, 104392 (2020).
51. Li, Z. et al. Investigating the mechanism and prevention of coal mine dynamic disasters by using dynamic cyclic loading tests. *Saf. Sci.* **115**, 215–228 (2019).
52. Xie, H., Ju, Y. & Dong, Y. Discussion of the "modulus of elasticity method" in the definition of classical damage. 2–6 (1997).
53. Amaral, P. M., Cruz Fernandes, J. & Guerra Rosa, L. Weibull statistical analysis of granite bending strength. *Rock Mech. Rock Eng.* **41**, 917–928 (2008).
54. Cheng, B. *Study on Damage and Failure Mechanism of Fractured Sandstone Based on Energy Dissipation and Release Principle* (Chongqing Jiaotong University, 2020).

Author contributions
Z.C.: Writing-original draft. S. D.: Writing-review & editing, Data curation. C. W.: Funding acquisition, Investigation. M. S.: Data curation. T. W.: Data curation. Q.C.: Investigation.

Funding
This work was supported by the National Natural Science Foundation of China (No.42567025, 52364004, 52264006), Guizhou Provincial Basic Research Program (Natural Science) (No.ZK[2024]011), Introduces talents for scientific research projects of Guizhou University (No. [2023]32), Basic Research Project of Guizhou University (No. [2023] 41), Guizhou Graduate Innovation Fund (No.2024YJSKYJJ064), Laboratory Open Project of Guizhou University (No. SYSKF2025-099), The Guizhou Provincial Science and Technology Foundation (No.GCC[2022]005-1).

Declarations

Competing interests
The authors declare no competing interests.

Additional information
Correspondence and requests for materials should be addressed to S.D.

Reprints and permissions information is available at www.nature.com/reprints.

Publisher's note Springer Nature remains neutral with regard to jurisdictional claims in published maps and institutional affiliations.

Open Access This article is licensed under a Creative Commons Attribution-NonCommercial-NoDerivatives 4.0 International License, which permits any non-commercial use, sharing, distribution and reproduction in any medium or format, as long as you give appropriate credit to the original author(s) and the source, provide a link to the Creative Commons licence, and indicate if you modified the licensed material. You do not have permission under this licence to share adapted material derived from this article or parts of it. The images or other third party material in this article are included in the article's Creative Commons licence, unless indicated otherwise in a credit line to the material. If material is not included in the article's Creative Commons licence and your intended use is not permitted by statutory regulation or exceeds the permitted use, you will need to obtain permission directly from the copyright holder. To view a copy of this licence, visit http://creativecommons.org/licenses/by-nc-nd/4.0/.

© The Author(s) 2025